

## Vortex-Induced Vibration of Two-Dimensional Isotoxal-Star Elements for Enhanced Wind Energy Harvesting

Y.J. Lee<sup>1</sup>, G. Zhou<sup>1</sup>, D. Estruch-Samper<sup>1</sup> and K.B. Lua<sup>2</sup>

<sup>1</sup>Department of Mechanical Engineering  
 National University of Singapore, Singapore 117575, Republic of Singapore

<sup>2</sup>Department of Mechanical Engineering  
 National Chiao Tung University, Hsinchu, Taiwan 30010, ROC

### Abstract

An investigation into the efficiency of two-dimensional polygonal structures undergoing transverse vortex-induced-vibration (VIV) is presented. The study aims at enhancing the yield in high oscillation amplitude for effective energy harvesting, for elements with a mass ratio of  $\approx 25$ , subjected to laminar cross-flow at Reynolds number of  $\approx 150$ . The efficiency of an isotoxal-star element with octagonal geometry is numerically investigated and compared to canonical circular cylinders. Under static conditions, the isotoxal-star element yields higher magnitude of fluctuating transverse force compared to the circular cylinders. When undergoing VIV at zero structural damping, the two cylinders have almost identical maximum oscillation amplitude despite the difference in the vortex strength and transverse force. Further investigations using an isotoxal-star element with diamond geometry and a triangular element suggests that VIV amplitude at zero structural damping is predominately governed by the magnitude of transverse drag force of the cross-section. At a structural damping ratio of 0.10, VIV enhancement due to changes in cross-sectional geometry becomes more apparent. Results suggest that VIV amplitude under damped condition is dependent on both the magnitude of fluctuating transverse force and the magnitude of transverse drag force. The two forces play different roles with regards to VIV response: a higher magnitude of fluctuating transverse force from a stronger von Karman vortex trail fosters the initiation of VIV. Conversely, strong transverse drag originating from the strong vorticity generated during transverse motions reduces the VIV. As such, VIV enhancement is a consequence of streamwise velocity or crossflow, while conversely, its reduction is primarily attributed to stronger transverse velocities. Results therefore suggest that enhanced VIV response could be potentially obtained through tailoring of the cross-sectional area to yield increased fluctuating transverse force while minimising transverse drag, represented here by the triangular element. Yet the compromise with regards to maintaining an effective omnidirectional performance of the elements renders isotoxal-star structures with multiple vertices (hereby assumed octagonal) more suitable for practical energy harvesting applications.

### Introduction

Vortex-induced vibration (VIV) of an elastically-mounted rigid circular cylinder in cross-flow has been explored extensively in literature [1,2]. In brief, an elastically mounted bluff body exposed to a steady uniform flow may be excited by its shed vortices and experience vortex-induced oscillations. As flow velocity increases, the VIV amplitude at low mass ratio exhibits three response branches, namely, the initial branch where the response amplitude increases with reduced velocity, followed by the upper branch which yields the maximum response amplitude, and the lower branch with a low response amplitude. Conversely, VIV at high mass ratio exhibits only two response branches, namely, the initial branch and the lower branch. The

different response branches yield distinct wake structures. The initial branch yields the 2S mode characterised by the shedding of two single vortices per cycle, which resembles the classical von Karman vortex trail. The upper and lower branches yield the 2P mode, comprising of two pairs of vortices per cycle.

This study is motivated by the recent interest in applying VIV for energy harvesting [3,4]. We aim to determine if cylinders with isotoxal-star cross-sections are able to induce stronger flow separation and yield enhanced VIV response amplitude compared to canonical circular cylinders. To that end, we compare the one degree-of-freedom VIV response of the circular cylinder to an isotoxal-star cylinder with octagonal geometry (henceforth referred to as “Star-8”). In addition, to aid in elucidating the mechanisms that govern VIV response, we studied the VIV of an isotoxal-star cylinder with diamond geometry (“Star-4”) and a triangular cylinder. The cross-sections are shown in Figure 1, in which the  $x$ -axis indicates the streamwise direction and the  $y$ -axis indicates the transverse direction.

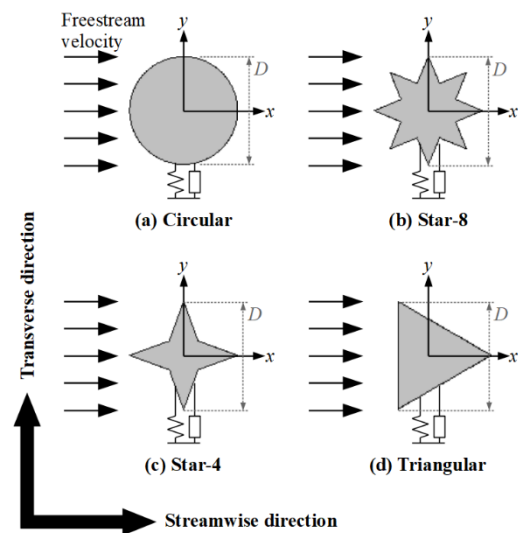


Figure 1. Schematic drawings of the cross-sectional geometries.

### Problem Definition

In this two-dimensional (2D) numerical study, a constant Reynolds number of 150 is imposed. Reynolds number is defined here as  $Re=UD/\nu$ , in which  $U$  is the cross-flow or freestream velocity,  $D$  is the cylinder diameter, and  $\nu$  is the fluid kinematic viscosity. This choice of  $Re$  is made in accordance to [5,6], in which the transition from 2D to 3D vortex shedding occurs above  $Re=150$ . Operating at  $Re=150$ , which is below transition, confers validity to our 2D numerical method.

Each cross-sectional geometry is first characterised by simulating the cylinder in cross-flow under static conditions, in which the cylinder position is fixed (i.e. without VIV). Static

simulations yield the Strouhal number,  $St=f_v D/U$ , in which  $f_v$  is the vortex shedding frequency. The root-mean-square of the fluctuating transverse force coefficient (RMS  $C_L'$ ) is computed based on equation (1).

Additionally, preliminary simulations show that the transverse drag force generated by the cross-section when it undergoes VIV acts against the VIV motion and may significantly impact the VIV response (see Figure 1 for definition of transverse direction). During actual VIV, the transverse drag force is a function of the instantaneous transverse velocity, which is not known *a priori*. Here, for the purpose of quantifying the resistance encountered by each cross-section when undergoing transverse motion, we adopt a quasi-steady analysis, whereby static simulations are used to quantify the transverse drag coefficient,  $C_{D,t}$  (equation (2)). The transverse drag force ( $F_{D,t}$ ) is the drag force (in the  $y$ -direction, see Figure 1) generated when each cross-section encounters a transverse incoming velocity (i.e. freestream velocity is in the  $y$ - instead of the  $x$ -direction, see Figure 1). Note that these simulations with the freestream velocity in the transverse ( $y$ ) direction are used only to quantify  $C_{D,t}$ .

$$C_L = F_L / (0.5\rho DU^2) \quad (1)$$

$$C_{D,t} = F_{D,t} / (0.5\rho DU^2) \quad (2)$$

Thereafter, a series of VIV simulations are conducted, with the freestream velocity acting in the longitudinal ( $x$ ) direction. Each cylinder undergoes one degree-of-freedom VIV as a mass-spring-damper system, governed by equation (3) in which  $m$ ,  $c$ , and  $k$  refer to the cylinder mass, structural damping coefficient, and spring stiffness, respectively.

$$m\ddot{y} + c\dot{y} + ky = F_L \quad (3)$$

To ensure fair comparison,  $k$  for each cylinder is set such that the natural frequency,  $f_N$  (given by equation (4)), is equal to  $f_v$  obtained from the static simulations. Consequently, the reduced velocity ( $U^*=U/f_N D$ ) is given by  $U^*=1/St$ . Both undamped and damped conditions are considered. Under the undamped condition, the structural damping ratio ( $\zeta$ , given by equation (5)) is zero; under the damped condition,  $\zeta=0.10$  is imposed. A moderate mass ratio (ratio of solid mass to displaced fluid mass) of  $m^*=25$  is implemented for the case of the circular cylinder. This represents an intermediate value between the low  $m^*=2.4$  to 20.6 used by Khalak and Williamson [7] and the high  $m^*\approx 250$  used by Feng [8].

$$f_N = \frac{1}{2\pi} \sqrt{\frac{k}{m}} \quad (4)$$

$$\zeta = \frac{c}{2\sqrt{mk}} \quad (5)$$

## Methodology

Numerical simulations are conducted using ANSYS FLUENT, Release 16. Spatial and temporal discretisations are second order accurate. The computational domain, depicted in Figure 2(a), is terminated by a constant velocity inlet, a zero gauge pressure outlet, and the symmetry boundary condition. The cylinder is modelled as a non-slip wall. The unstructured mesh comprises of triangular elements and two layers of wall-adjacent rectangular elements, which amount to about 38 thousand elements when grid convergence is achieved. A dynamic mesh scheme is implemented, in which the inner region is rigid, and the outer region undergoes spring-like deformation while the outer boundaries are stationary.

VIV of the mass-spring-damper system (see equation (3)) is implemented by the algorithm shown in Figure 3, in which  $dt$  is the computational time step. An under-relaxation factor of

$\alpha=0.5$  is present to aid numerical stability. VIV simulations are conducted over a duration of  $500T$ , in which  $T$  is the non-dimensional time unit ( $T=D/U$ ). The normalised maximum oscillation amplitude ( $A^*_{max}=A_{max}/D$ ) is sampled from  $400T$  to  $500T$ , during which the flow is in periodic state.  $A_{max}$  represents the maximum achievable VIV displacement for a given scenario.

The simulation method is validated by comparing with previous simulation results [9,10] (Figure 2(b)). Good agreement between past and present results demonstrate the reliability of our VIV method. Note that the slight deviation from [10] is due to streamwise oscillation being included in [10].

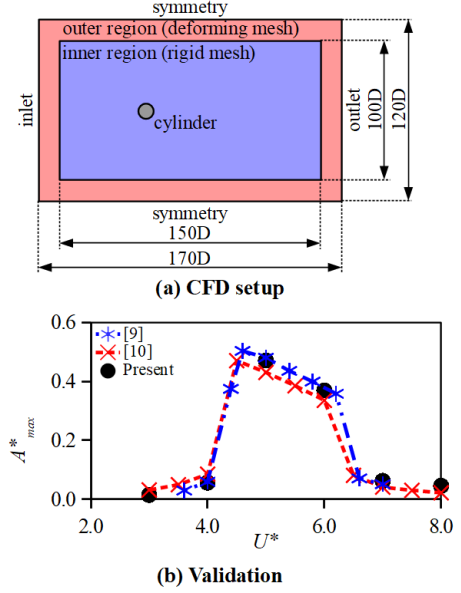


Figure 2. (a) Computational setup and (b) validation results.

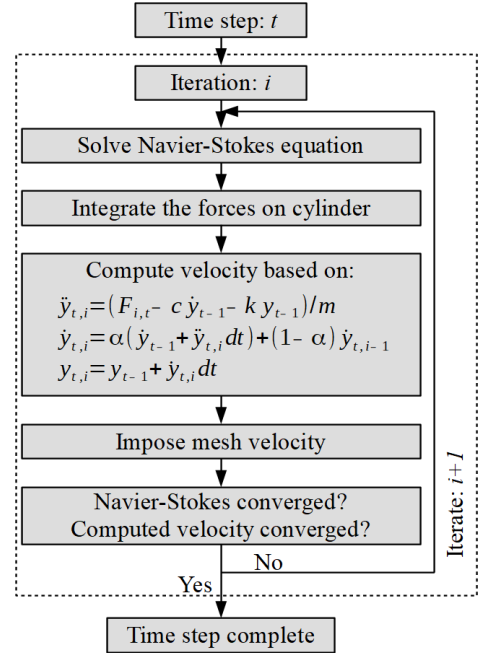


Figure 3. VIV algorithm.

## Results

Static simulations yield RMS  $C_L'$  and mean  $C_{D,t}$ , which are plotted in Figure 4 alongside the RMS  $C_L'$ /mean  $C_{D,t}$  ratio.  $St$  for the circular, Star-8, Star-4, and triangular cylinders are

0.182, 0.187, 0.179, and 0.162, respectively; these values determine the appropriate  $k$  for the VIV simulations. At this juncture, we need to define the cylinder mass ( $m$ ) for the different geometries, as  $f_N$  is dependent on  $m$ . There are two feasible criteria for determining  $m$ ; one can either maintain constant  $m^*$ , which imposes constant cylinder density, or opt to maintain constant cylinder mass,  $m$ . This choice is significant because the cross-sectional area of the non-circular cylinders differ from that of the circular cylinder. To investigate whether constant  $m^*$  or  $m$  yields fairer comparison, we take the circular cylinder as the baseline case and compare its  $A^*_{max}$  against those of the Star-8 cylinder. Two different scenarios are presented, namely, the “Star-8D” scenario in which constant  $m^*$  is imposed, and the “Star-8M” scenario in which  $m$  is constant.

Figure 5 shows the  $A^*_{max}$  for the circular, Star-8D, and Star-8M cylinders. At  $\zeta=0.00$ , the three cases yield nearly identical  $A^*_{max}$ . It is interesting to note that despite the 24% increase in RMS  $C_L'$  of the Star-8 cylinder over that of the circular cylinder, this increase is not necessarily reflected in the  $A^*_{max}$  results. Furthermore, at  $\zeta=0.00$ , the mass property has little effect on  $A^*_{max}$  as evidenced by the Star-8D and Star-8M cylinders yielding almost identical response amplitude. This is because both the mass-damping parameter ( $m^*\zeta$ ) and Skop-Griffin parameter ( $S_G=2\pi^3St^2m^*\zeta$ ), which are the primary parameters governing VIV amplitude [2], take on the value of zero at  $\zeta=0.00$  regardless of the cylinder mass. Hence, cylinder mass does not significantly affect  $A^*_{max}$  at zero structural damping.

Under the damped condition ( $\zeta=0.10$ ), the effect of cylinder mass becomes more apparent. The Star-8D cylinder shows a considerably increase of 108% in  $A^*_{max}$  over the circular cylinder. This contrasts with the  $A^*_{max}$  of the Star-8M cylinder, which is only 11% higher than the circular cylinder. The significant increase in  $A^*_{max}$  of the Star-8D cylinder can be attributed to the 47% decrease in cross-sectional area and the corresponding decrease in cylinder mass compared to the circular cylinder. The preceding results strongly suggest that maintaining constant  $m$ , rather than  $m^*$ , is a more appropriate criteria for comparing the VIV enhancement of different cross-sections. Consequently, the constant  $m$  criterion has been adopted for the remainder of this study.

The main objective of this study is to determine if isotoxal-star cross-section enhances VIV response for energy harvesting applications. Considering that the conversion of mechanical to electrical energy inevitably results in a significant amount of damping, we focus on the circular and Star-8M cylinders at  $\zeta=0.10$  (Figure 5). The isotoxal-star element, represented here by Star-8M, does provide a small but noticeable enhancement in VIV amplitude. Evidently, a cross-sectional geometry that induces stronger vortex formation, as indicated by the increase in RMS  $C_L'$ , does not necessarily increase VIV amplitude at the commensurate magnitude. This can be attributed to two counter-rotating mechanisms that are present. Firstly, the von Karman vortex trail generated by the isotoxal-star element is relatively stronger, resulting in higher magnitude of fluctuating transverse force and hence fostering the initiation of VIV effect. However, strong vorticity is also generated during transverse motions and this in turn prompts the associated transverse drag to reduce the VIV. As such, VIV enhancement is a consequence of streamwise velocity or crossflow, while conversely, its reduction is primarily attributed to transverse velocities. It follows that cross-sectional geometry that yields strong von Karman vortices while maintaining low transverse drag may be more ideal for enhancing VIV response.

To test the preceding hypothesis, we conducted additional simulations using the Star-4 and triangular cylinders (see Figure 1) at  $\zeta=0.00$  and 0.10; the results are plotted alongside those of

the circular and Star-8M cylinders in Figure 6. Under the undamped condition ( $\zeta=0.00$ ), the circular, Star-8, and triangular cylinders yield comparable  $A^*_{max}$ ; conversely,  $A^*_{max}$  of the Star-4 cylinder is significantly lower. Under the damped condition ( $\zeta=0.10$ ),  $A^*_{max}$  increases in the order of: circular, Star-8, Star-4, and triangular cylinder.

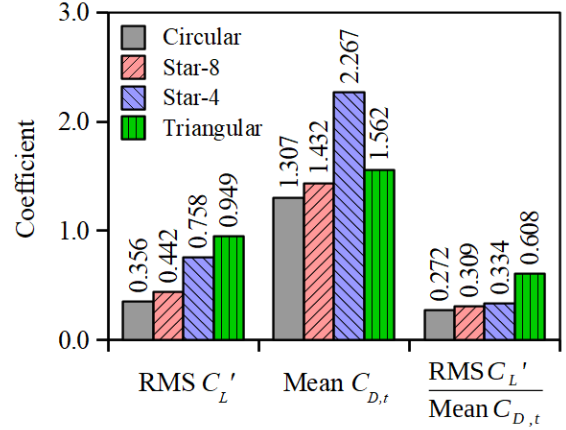


Figure 4. Force coefficients of static cylinders in cross-flow.

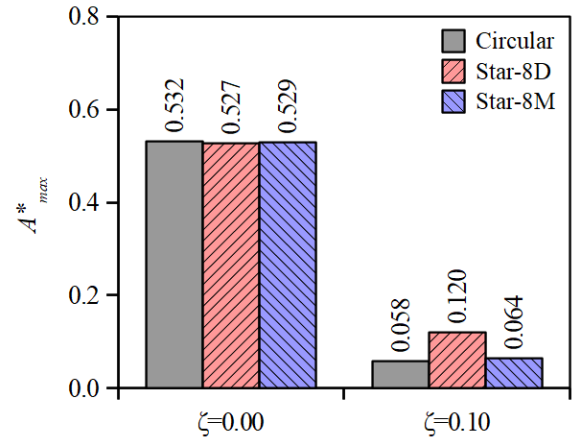


Figure 5. Response amplitude of the circular, Star-8D, and Star-8M cylinders in VIV.

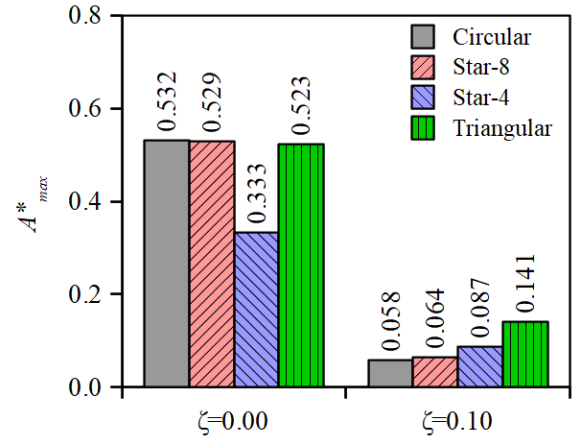


Figure 6. Response amplitude of the circular, Star-8, Star-4, and triangular cylinders of equal cylinder mass.

We note two correlations between the VIV response of the different cylinders and their respective force coefficients under static conditions. First, under the undamped condition ( $\zeta=0.00$ ), the  $A^*_{max}$  trend (Figure 6) shows an inverse correlation with the trend of mean  $C_{D,t}$  shown in Figure 4. Specifically, the circular,

Star-8, and triangular cylinders, which yield comparable  $A^*_{max}$ , have comparable mean  $C_{D,t}$ . Conversely, the Star-4 cylinder has significantly higher mean  $C_{D,t}$  (Figure 4) which is associated to the decrease in  $A^*_{max}$ . This suggests that, at very low structural damping ratio, VIV response may be governed by the magnitude of transverse drag. Second, at the structural damping ratio of  $\zeta=0.10$ ,  $A^*_{max}$  (Figure 6) can be correlated to the RMS  $C_L$ /mean  $C_{D,t}$  ratio in Figure 4, which increases in the same order. This suggests that, at high structural damping ratio, both the magnitude of the fluctuating transverse force and transverse drag determine the VIV response.

As per our preceding postulation, it is apparent that the triangular cylinder, by virtue of its high RMS  $C_L$ /mean  $C_{D,t}$  ratio, yields significantly enhanced VIV response over that of the circular cylinder (Figure 6). However, tailoring the cross-section for high RMS  $C_L$ /mean  $C_{D,t}$  ratio tends to result in a compromise in terms of maintaining an omni-directional performance. For example, the triangular cross-section is highly sensitive to incoming flow direction, which lowers its practicality for omni-directional wind energy harvesting. Hence, isotoxal-star structures with multiple vertices (represented here by the octagonal shape) remains more suitable for our application, which rely on continued low-speed wind energy harvesting with minor sensitivity to flow direction.

Figure 8 shows the wake structures of the four different cross-sections, which are visualised by the contours of normalised vorticity ( $\omega^*=\omega D/U$ ). The 2S mode is clearly observed, which is expected for our moderate mass ratio of  $m^*\approx 25$ . The difference in cross-sectional geometry mainly affects the near-field vorticity distribution, with limited effect on the general wake topology.

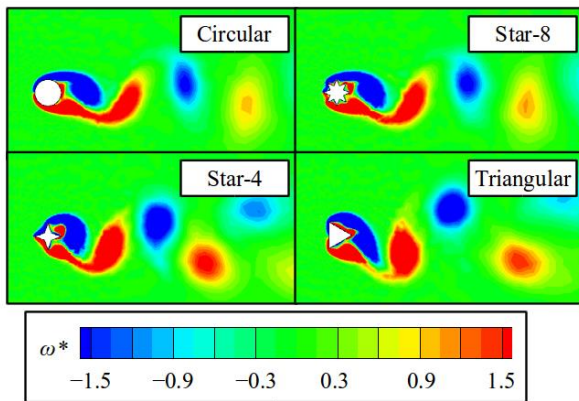


Figure 7. Contours of normalised vorticity of different geometries undergoing VIV at  $\zeta=0.10$ , taken at peak positive displacement.

## Conclusions

Numerical investigation has been conducted on the effect of cross-sectional geometry on the one-degree-of-freedom VIV response of a cylinder in cross-flow, focusing on the potential benefits of isotoxal-star elements in wind energy harvesting applications. The effect of cross-sectional geometry on the VIV response amplitude is dependent on structural damping. Results suggest that when structural damping is negligible ( $\zeta=0.00$ ), the mean transverse drag coefficient of the cross-section determines the response amplitude; low transverse drag is associated with high response amplitude. Conversely, at higher structural damping ratio of  $\zeta=0.10$ , response amplitude increases with the ratio of fluctuating transverse force to the mean transverse drag. Present results indicate that the isotoxal-star element, assumed here to be octagon, yields slightly enhanced VIV response over that of the canonical circular

cylinder at high structural damping. Further enhancements to VIV response by tailoring the cross-sectional geometry for high fluctuating transverse force and low transverse drag inevitably compromises the omni-directional property of the cylinder, which lowers its utility for omni-directional wind energy harvesting.

Additionally, investigation of cylinders with different mass properties reveals that maintaining constant cylinder mass yields more comparable response amplitudes than tests conducted with constant cylinder density or mass ratio,  $m^*$ . This suggests that the conventional  $m^*$  definition (ratio of solid mass to displaced fluid mass) may not be the most appropriate under certain circumstances. An alternative definition may be worth exploring.

## Acknowledgments

This research is supported by the Ministry of Education, Singapore Academic Research Fund (AcRF) FRC Tier 1 Grant (R-265-000-585-114).

## References

- [1] Sarpkaya, T.A. A Critical Review of the Intrinsic Nature of Vortex-Induced Vibrations, *Journal of Fluids and Structures*, **19**, 2004, 389-447.
- [2] Williamson, C.H.K. & Govardhan, R. Vortex-Induced Vibrations, *Annual Review of Fluid Mechanics*, **36**, 2004, 413-455.
- [3] Bernitsas, M.M., Raghavan, K., Ben-Simon, Y. & Garcia, E.M. VIVACE (Vortex Induced Vibration Aquatic Clean Energy): A New Concept in Generation of Clean and Renewable Energy from Fluid Flow, *Journal of Offshore Mechanics and Arctic Engineering*, **130**, 2008, 041101.
- [4] Zhao, L. & Yang, Y. Toward Small-Scale Wind Energy Harvesting: Design, Enhancement, Performance Comparison, and Applicability, *Shock and Vibration*, 2017, 3585972.
- [5] Norberg, C. *Effects of Reynolds Number and a Low-Intensity Freestream Turbulence on the Flow Around a Circular Cylinder*, Chalmers University of Technology, 1987.
- [6] Sohankar, A., Norberg, C. & Davidson, L., Simulation of Three-Dimensional Flow Around a Square Cylinder at Moderate Reynolds Numbers, *Physics of Fluids*, **11**, 1999, 288-306.
- [7] Khalak, A. and Williamson, C.H.K., Investigation of Relative Effects of Mass and Damping in Vortex-Induced Vibration of Circular Cylinder, *Journal of Wind Engineering and Industrial Aerodynamics*, **69**, 1997, 341-350.
- [8] Feng, C.C. *The Measurement of Vortex Induced Effects in Flow Past Stationary and Oscillating Circular and D-Section Cylinders*, University of British Columbia, 1968.
- [9] Leontini, J.S., Thompson, M.C. & Hourigan, K. The Beginning of Branching Behaviour of Vortex-Induced Vibration During Two-Dimensional Flow, *Journal of Fluids and Structures*, **22**, 2006, 857-864.
- [10] Li, Z., Yao, W., Yang, K., Jaiman, R.K. & Khoo, B.C. On the Vortex-Induced Oscillations of a Freely Vibrating Cylinder in the Vicinity of a Stationary Plane Wall, *Journal of Fluids and Structures*, **65**, 2016, 495-52